Search for production of dark fermion candidates in association with heavy neutral gauge boson decaying to dimuon in proton-proton collisions at $\sqrt{s}$ = 8 TeV using CMS open data*

Y. Mahmoud[1,2†] H. Abdallah[2] M. T. Hussein[2] S. Elgammal[1]

[1]Centre for theoretical physics, The British University in Egypt, Egypt
[2]Physics Department, Faculty of Science, Cairo University, Egypt

Abstract: In this study, we conducted a search for dark matter using a part of the data recorded by the CMS experiment during run-I of the LHC in 2012 with a center of mass energy of 8 TeV and an integrated luminosity of 11.6 fb^{-1}. These data were gathered from the CMS open data. Dark matter, in the framework of the simplified model (mono-Z'), can be produced from proton-proton collisions in association with a new hypothetical gauge boson, Z'. Thus, the search was conducted in the dimuon plus large missing transverse momentum channel. One benchmark scenario of mono-Z', which is known as light vector, was used for interpreting the CMS open data. No evidence of dark matter was observed, and exclusion limits were set on the masses of dark matter and Z' at 95% confidence level.

Keywords: dark matter, large hadron collider, CMS open data, search for new physics, dark fermion

DOI: 10.1088/1674-1137/ad20d5

I. INTRODUCTION

Several pieces of cosmological evidence, based on recent observations [1−4], have confirmed the existence of another type of invisible matter called dark matter (DM). These studies have also estimated the abundance of DM in the universe to be 27% of the total energy distribution in the universe.

Several theoretical models have been introduced to provide a description of the composition of DM. One of the proposed explanations is that DM consists of weakly interacting massive particles (WIMPs). The WIMP theory was successful in providing the correct value of observed density (WIMP miracle) [5].

Although the standard model (SM) of particle physics provides a decent explanation for the visible matter in the universe, it falls short in providing an explanation for the other type of invisible non-baryonic matter, i.e., DM. Therefore, alternative theories beyond the standard model (BSM) are needed to provide a DM candidate[6, 7].

The masses of DM candidates can range from a few GeV to a few TeV [8], which can be achieved at particle colliders such as the Large Hadron Collider (LHC). Many searches for DM candidates have been conducted by analysing data collected by the CMS experiment during RUN II. These searches rely on the production of a visible object "X" that recoils against the large missing transverse momentum from the DM particles leaving a signature of $X + \not{p}_T$ in the detector. The visible particle can be an SM particle, such as W, Z bosons or jets [9], a photon [10], or an SM Higgs boson [11].

The visible particle could also be a heavy neutral gauge boson (Z') predicted by BSM models [12, 13]. This type of models is known as the mono-Z' model [13]; it encompasses three possible scenarios that propose the production of DM accompanied by the Z' boson: dark Higgs scenario (DH), light vector scenario (LV), and light Z' with the inelastic effective field theory (EFT) scenario. Z' is neutral and can decay leptonically into a pair of oppositely charged leptons (l^+l^-) or hadronically into a pair of quarks leading to a dijet. Therefore, it can be detected as a resonance in the dilepton or dijet invariant mass distribution [14−17]. The hadronic decay of Z' in the mono-Z' portal was studied previously by the ATLAS collaboration in [18].

In a previous analysis [19], we considered the lepton-

Received 22 November 2023; Accepted 22 January 2024; Published online 23 January 2024

* Y. Mahmoud wishes to thank the Center for Theoretical Physics (CTP) at the British University in Egypt (BUE) for its continuous support, both financially and scientifically, for this work.

† E-mail: yehia.abdelaziz@bue.edu.eg

Content from this work may be used under the terms of the Creative Commons Attribution 3.0 licence. Any further distribution of this work must maintain attribution to the author(s) and the title of the work, journal citation and DOI. Article funded by SCOAP[3] and published under licence by Chinese Physical Society and the Institute of High Energy Physics of the Chinese Academy of Sciences and the Institute of Modern Physics of the Chinese Academy of Sciences and IOP Publishing Ltd

ic decay of Z'(i.e., $Z' \to \mu^+\mu^-$) for two of the aforementioned scenarios: Dark Higgs (DH) and inelastic effective field theory (EFT). The data sets used in this study were obtained from the CMS open data project [20], which released data sets from recorded and simulated proton-proton collisions at the centre of mass energy ($\sqrt{s} = 8$ TeV). These data sets are publicly available for all researchers even if they are not members of the CMS collaboration. The open data samples provide a great potential for researchers in high energy particle physics to test many theoretical models available in literature [21].

The analysis presented in the current paper is complementary to our aforementioned previous study [19]. In particular, we here present a search for dark fermions (DFs) originated from the LV scenario in events with dimuon with high invariant mass plus large missing transverse momentum. Similar searches for DM in this channel have been conducted for the ATLAS and CMS experiments at the LHC, with the visible particle being a Z boson decaying to dimuon at $\sqrt{s}$= 8 TeV [22] and $\sqrt{s}$ = 13 TeV [23].

Section II presents the theoretical formalism of the LV scenario and its free parameters. The simulation techniques used for event generation for the signal and SM background samples are reported in Section III, together with the description of CMS open data files from the proton-proton collisions. The selection cuts and analysis strategy are explained in Section IV. Finally, the results and summary of this analysis are discussed in Sections V and VI, respectively.

II. SIMPLIFIED MODEL

Our target model is known as mono-$Z'$and was discussed in [13]. It predicts the production of DM from proton-proton collisions at the LHC through a new heavy gauge boson, Z'. The process of DM production in the mono-Z'model follows one of three different possible scenarios: dark Higgs (DH), inelastic effective field theory coupling (EFT), which was studied in [19], and LV, which is illustrated in Fig. 1.

In the rest of this paper, the analysis is focused on the LV scenario, which is also know as DF according to [18]. The proposed DF can be produced through a process of pair annihilation of two quarks $q\bar{q}$ mediated by heavy vector boson Z', which then leads to two DFs: a light DF(χ_1) and a heavy one(χ_2). χ_2 is heavy enough to decay to Z' and another light DFχ_1 (i.e., $\chi_2 \to Z'\chi_1$), as shown in Fig. 1.

The interaction term in the Lagrangian between the DFs and Z' is given by [13]

$$\frac{g_{DM}}{2} Z'_\mu(\bar{\chi_2}\gamma^\mu\gamma^5\chi_1 + \bar{\chi_1}\gamma^\mu\gamma^5\chi_2),$$

where g_{DM} is the coupling of Z' with DFs χ_1 andχ_2.

Two assumption can be used to set the masses in the DF model. One with a heavy dark sector and the other with a light dark sector, as shown in Table 1, as proposed in [13]. In the case of the light dark sector case, given that the cross section increase with lower χ_1 mass, we include an optimistic case with a very light DF χ_1 = 1,5,...,50 GeV, while χ_2 is notably heavier than χ_1. For the case of the heavy dark sector, the DF masses scale with the mediator mass.

In the rest of this paper, the coupling of Z' with the visible fermions will be represented by g_{SM}, while the coupling of $Z'$with the DFs will be represented by g_{DM}. The only allowed decays in the DF scenario are assumed to be the decay of $Z' \to \chi_1\chi_2$, $\chi_2 \to Z'\chi_1$, and $Z' \to \mu\tilde{\mu}$. The total decay width of Z' and χ_2 can be calculated from the values of the masses of $Z'$and DFs as well as from the coupling constants.

The free parameters in this scenario are the lightest DF mass denoted by M_{χ_1}, the Z' mass denoted by $M_{Z'}$, and the coupling of Z' with both SM and DF particles denoted by g_{SM} and g_{DM}. The value taken for coupling constant g_{SM} is 0.1, given that a previous study [18] showed that g_{SM} was excluded from the interval between 0.13 and 0.26 for dimuon invariant mass above 200 GeV. The value of g_{DM} was set to be 1.0, following the recommendation of the LHC Dark Matter Working Group [24]. Meanwhile, the values of the masses are not fixed but scanned over.

The signature that these processes leave at the detector typically consists of two oppositely charged leptons or jets produced from the decay of Z', in addition to a large missing transverse momentum from stable DFs χ_1. This scenario was previously studied by the ATLAS collaboration [18] with a hadronically decaying Z'. In this study, we considered the muonic decay of on-shell Z' given that

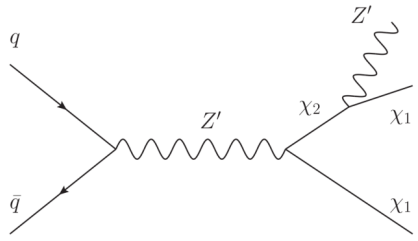

Fig. 1. Feynman diagrams for the DF scenario in the mono-Z' simplified model.

Table 1. Light and heavy mass assumptions for the dark sector in the DF scenario [13].

Scenario	Mass assumptions
Light dark sector	M_{χ_1} = 1,5,...,50 GeV
	$M_{\chi_2} = M_{\chi_1} + M_{Z'} + 25$ GeV
Heavy dark sector	$M_{\chi_1} = M_{Z'}/2$ GeV
	$M_{\chi_2} = 2M_{Z'}$ GeV

the CMS detector is optimized for this decay channel (which is a clean channel with respect to SM backgrounds). Thus, our studied events exhibit the following topology: $(\mu^+\mu^- + \not{p}_T)$. For the DF scenario, using the light dark sector case, Table 2 reports the cross section times branching ratios calculated for different sets of Z' and χ_1 masses. As we can see from this table, the cross section is sensitive to the change in the DF mass. The simulated DF signals used in this analysis are private production samples for which we used the matrix element event generator MadGraph5 aMC@NLO v2.6.7 [25]. We are grateful to Tongyan Lin and co-authors [13] for sharing the so-called Universal FeynRules Output (UFO) for the mono-Z′ model. In the rest of this paper, we will consider the light dark sector scenario and neglect the heavy case, because the cross section times branching ratio calculations presented in Table 3 for the heavy dark sector are much lower (over a factor of 10) than those for the light case. Hence, this analysis does not include any sensitivity to the heavy dark sector scenario.

III. DATA AND SIMULATED SAMPLES

A. CMS detector and reconstructed objects

The Compact Muon Solenoid is one of the four main experiments built to study the proton-proton collision data collected at the LHC. Located at one of the collision points of the LHC, its main objective is the search for new physics beyond the standard model. The CMS is made of several concentric layers of sub-detectors, each used for detection of a different type of particle. The CMS was designed to provide a proper identification of electrons, photons, hadrons, muons, and jets as well as measure their energy and momentum. The technical design of the CMS detector makes it possible to have a good measurement of the missing transverse momentum. A precise measurement of the muon momentum requires a strong magnetic field; a super conducting solenoid is used for this purpose.

The coordinate system of the CMS was designed for the origin to be located at the collision point. The x-axis extends radially from the beamline, the y-axis ascends vertically, and the z-axis follows the beam's trajectory. The azimuthal angle (ϕ) describes the particle's angular orientation around the beamline, typically measured in radians. Finally, the pseudorapidity (η), expressed in terms of the polar angle (θ), is defined as $\eta = -\ln[\tan(\theta/2)]$. Thus, it is possible to calculate the transverse momentum (p_T) and transverse energy (E_T) from the x and y components of the momentum.

The inner most layer of the detector is the inner tracker, which is used to measure the momenta of charged particles. The second layer is the electromagnetic calorimeter (ECAL), which is designed for accurately identifying electrons and photons and measuring their energies. The third layer is the hadron calorimeter (HCAL), which detects and measures the energy of hadrons. The super conducting magnet constitutes the fourth layer; it provides a magnetic field of 3.8 T that bends the paths of high energy charged particles, allowing the measurement of their momenta. The outermost layer of the detector is the muon system, which uses three types of detectors: drift tubes (DT) in the barrel part of the detector, cathode strip champers (CSC) in the endcaps, and resistive plate champers (RPC) to complete both the barrel part and endcaps.

Given that our study includes muons and missing transverse energy in the final state, we next describe how they are reconstructed. The muon objects are identified and reconstructed by fitting muon tracks from both the inner tracker and muon system [26, 27]. The missing trans-

Table 2. DF cross section times branching ratios (in pb) calculated for different sets of masses M_{χ_1} (in GeV) and $M_{Z'}$ (in GeV), and for the light dark sector mass assumption with the following couplings constants: $g_{SM} = 0.1$, $g_{DM} = 1.0$ at $\sqrt{s} = 8$ TeV.

M_{χ_1}	$M_{Z'}$									
	150	200	250	300	350	400	450	500	600	700
1	9.40×10^{-2}	4.37×10^{-2}	2.28×10^{-2}	1.307×10^{-2}	0.765×10^{-2}	0.454×10^{-2}	0.294×10^{-2}	0.199×10^{-2}	0.98×10^{-3}	0.52×10^{-3}
5	7.50×10^{-2}	3.58×10^{-2}	1.908×10^{-2}	1.104×10^{-2}	0.655×10^{-2}	0.392×10^{-2}	0.255×10^{-2}	0.172×10^{-2}	0.85×10^{-3}	0.46×10^{-3}
10	5.75×10^{-2}	2.84×10^{-2}	1.54×10^{-2}	0.909×10^{-2}	0.545×10^{-2}	0.327×10^{-2}	0.215×10^{-2}	0.145×10^{-2}	0.73×10^{-3}	0.39×10^{-3}
15	4.51×10^{-2}	2.282×10^{-2}	1.26×10^{-2}	0.757×10^{-2}	0.46×10^{-2}	0.278×10^{-2}	0.184×10^{-2}	0.126×10^{-2}	0.63×10^{-3}	0.34×10^{-3}
20	3.59×10^{-2}	1.86×10^{-2}	1.04×10^{-2}	0.637×10^{-2}	0.391×10^{-2}	0.237×10^{-2}	0.158×10^{-2}	0.108×10^{-2}	0.556×10^{-3}	0.03×10^{-3}
25	2.89×10^{-2}	1.53×10^{-2}	0.879×10^{-2}	0.541×10^{-2}	0.334×10^{-2}	0.205×10^{-2}	0.137×10^{-2}	0.95×10^{-3}	0.488×10^{-3}	0.26×10^{-3}
30	2.35×10^{-2}	1.27×10^{-2}	0.743×10^{-2}	0.462×10^{-2}	0.289×10^{-2}	0.178×10^{-2}	0.12×10^{-2}	0.83×10^{-3}	0.434×10^{-3}	0.23×10^{-3}
35	1.94×10^{-2}	1.07×10^{-2}	0.633×10^{-2}	0.398×10^{-2}	0.251×10^{-2}	0.155×10^{-2}	0.105×10^{-2}	0.742×10^{-3}	0.385×10^{-3}	0.213×10^{-3}
40	1.61×10^{-2}	0.909×10^{-2}	0.543×10^{-2}	0.343×10^{-2}	0.218×10^{-2}	0.137×10^{-2}	0.936×10^{-3}	0.657×10^{-3}	0.343×10^{-3}	0.192×10^{-3}
50	1.14×10^{-2}	0.66×10^{-2}	0.407×10^{-2}	0.26×10^{-2}	0.16×10^{-2}	0.106×10^{-2}	0.739×10^{-3}	0.371×10^{-3}	0.278×10^{-3}	0.157×10^{-3}

Table 3. Cross section times branching ratio (in pb) for the heavy dark sector in the DF scenario calculated for different sets of masses $M_{Z'}$ with the following couplings constants: $g_{SM} = 0.1$, $g_{DM} = 1.0$ at $\sqrt{s} = 8$ TeV.

$M_{Z'}$/GeV	$\sigma \times$BR /pb
150	1.73×10^{-2}
200	0.51×10^{-2}
250	0.18×10^{-2}
300	0.74×10^{-3}
350	0.32×10^{-3}
400	0.14×10^{-3}
450	0.69×10^{-4}
500	0.36×10^{-4}
600	0.11×10^{-4}
700	0.33×10^{-5}

verse momentum is reconstructed according to the particle flow (PF) algorithm described in [28]. The PF algorithm calculates the missing momentum from the imbalance in the vector sum of the momenta in the transverse plane. Many factors can affect the magnitude of $\vec{\not{p}}_T$, leading to the overestimation or underestimation of its true value. These factors include the calorimeter response as well as minimum energy thresholds in the calorimeter and p_T thresholds, inefficiencies in the tracker, and non-linearity of the response of the calorimeter for hadronic particles [29].

To account for the effect of these factors, we replace $\vec{\not{p}}_T$ by its corrected version $\not{p}_T^{\rm corr}$, which is one of the variables included in the particle flow (PF) MET object [30, 31] in the CMS software [32].

B. Monte Carlo simulation of the LV scenario

The signal samples for the LV scenario were generated using MadGraph5_aMC@NLOv2.6.7 [25] and the hadronization provided by Pythia [33]. We produced several samples for the signal at different sets of masses of DF χ_1 and mediator Z', and calculated their cross sections. The mass of Z' ranged from 150 GeV to 700 GeV. For DF Z', the mass ranged from 1 GeV to 50 GeV. The couplings were assumed to be $g_{SM} = 0.1$ and $g_{DM} = 1.0$.

The detector simulation of the readout system response (digitization) and reconstruction processes were performed using the standard CMS open data software framework [32] (release CMSSW_5_3_32) at $\sqrt{s} = 8$ TeV, with the suitable trigger list used for CMS-2012 analysis. The effect of pile-up was simulated by overlaying MC generated minimum bias events [34].

C. Background estimation

The three SM background processes yielding lepton pairs in the signal region are the production of top quark pairs ($t\bar{t}$), Drell-Yan (DY) production, and production of diboson (WW, WZ and ZZ). The second type of background is the jet background, which originates from the misidentification of jets as muons, where a jet or multijet passes the muons selection criteria. This type of backgrounds originates from two processes: W+jet and QCD multijet. The contamination of single and multijet backgrounds in data is usually estimated from data using a data driven method [35]. The third is the cosmic muon background [35].

For simulating background processes, we used the CMS open MC samples at $\sqrt{s}$= 8 TeV [36]. DY background $q\bar{q} \to \mu\bar{\mu}$ was generated using the POWHEGBoxv1.0 MC program [37, 38] interfaced with Pythia v.6.4.26 for the parton shower model [33]. Another important source of SM backgrounds with dimuon and missing p_T in the final state is the fully leptonic decay of $t\bar{t}$, which was generated using MadGraph5_aMC@NLO [25]. The electroweak diboson production channels as WW and WZ were generated with MadGraph interfaced with Pythia v.6.4.26, and ZZ for four muons process also generated with POWHEGBoxv1.0. The Monte Carlo samples and their corresponding cross sections used in this analysis, and calculated at next-to-leading order (NLO) or next-to-next-to-leading order (NNLO), are listed in Table 4.

The contributions of the SM background processes were estimated from the Monte Carlo simulations following the same method applied in a previous search for new resonance within the dimoun events at $\sqrt{s} = 8$ TeV [35]. The Monte Carlo samples of the SM backgrounds, listed in Table 5, were normalized to their corresponding cross sections.

Note that the contribution of the jets background is very small above 400 GeV in the dimuon invariant mass spectrum, as estimated in [35], with only 3 events misidentified as muons for an integrated luminosity of 20.6 fb^{-1}. Thus, in our case (luminosity = 11.6 fb^{-1}), this contribution is expected to be much lower than 3 events. Meanwhile, for a mass bin of [120−400] GeV, the jets misidentification was estimated to be 147 events, which represents approximately 0.15% of the total SM backgrounds (96800 events) estimated in this mass bin [35]; its impact on our results is very small. For these reasons, the QCD and W+jets backgrounds estimated from data are negligible in the current study.

IV. SELECTION OF EVENT AND SYSTEMATIC UNCERTAINTIES

To select events of interest, a selection criterion was designed to choose events with two high p_T muons and large missing transverse momentum resulting from the DF candidate. The selection criterion is as follows. Both

Table 4. Data sets and their names used for the simulation of the SM backgrounds for proton-proton collisions at $\sqrt{s} = 8$, obtained from the CMS open MC samples, and their corresponding cross sections and order of calculation.

Process	Generator	Data Set Name	$\sigma \times$BR(pb)	Order
DY($\mu\bar{\mu}$)	POWHEG	DYToMuMu_M-20_CT10_TuneZ2star_v2_8TeV. [39]	1916 [21]	NNLO
$t\bar{t}$ + jets	MADGRAPH	TTJets_FullLeptMGDecays_8TeV. [40]	23.89 [41]	NLO
WW + jets	MADGRAPH	WWJetsTo2L2Nu_TuneZ2star_8TeV. [42]	5.8 [21]	NLO
WZ + jets	MADGRAPH	WZJetsTo3LNu_8TeV_TuneZ2Star. [43]	1.1 [21]	NNLO
$ZZ \to 4\mu$	POWHEG	ZZTo4mu_8TeV. [44]	0.077 [21]	NLO

Table 5. The CMS-2012 open data samples used in this analysis and the corresponding integrated luminosity.

Run	Data Set	$\mathcal{L}$ (fb^{-1})
Era B	SingleMu/Run2012B-22Jan2013-v1/AOD.[45]	11.6 [46]
Era C	SingleMu/Run2012C-22Jan2013-v1/AOD.[47]	

muons should pass the high (p_T) muon identification introduced in [48, 49] and satisfy the following preliminary selection:

- p_T^{μ}(GeV) > 45,
- η^{μ}(rad) < 2.1.

Thus, the events that were selected are those with two oppositely charged muons in which at least one of them passed the single muon trigger HLT_Mu40_eta2p1. This same selection was applied for the search for new physics in 2012 analysis concerning events containing dimuon resonance. We restricted the mass of the dimuon to be over 80 GeV, given that the Z' mass regime lies above this.

Figure 2 shows the distribution of the missing transverse momentum after the preliminary selection; the CMS open data are represented by black dots with error bars (statistical error only), the cyan histogram represents the Drell-Yan background, the grey histogram represents the vector boson pair backgrounds (WW, WZ, and ZZ), and the red histogram represents the $t\bar{t}$+ jets background. These histograms are stacked; the signal of DF scenario was generated with an invariant mass of the neutral gauge boson, $Z'(M_{Z'} = 300$ GeV), and the mass of the DF ($M_{\chi_1} = 1$ GeV), represented by the blue colored line, is overlaid. The total systematic uncertainty (explained in Section IV) is included in the ratio plot along with the statistical uncertainties. This figure exhibits good agreement between the data points and simulated SM backgrounds within the statistical and systematic uncertainties.

Given that the selected signal events, represented by the blue solid line in Fig. 2, are embedded in the background, we need to apply a tighter selection in order to discriminate the signal from the SM backgrounds, as explained next.

In addition to the preliminary selection, extra tighter

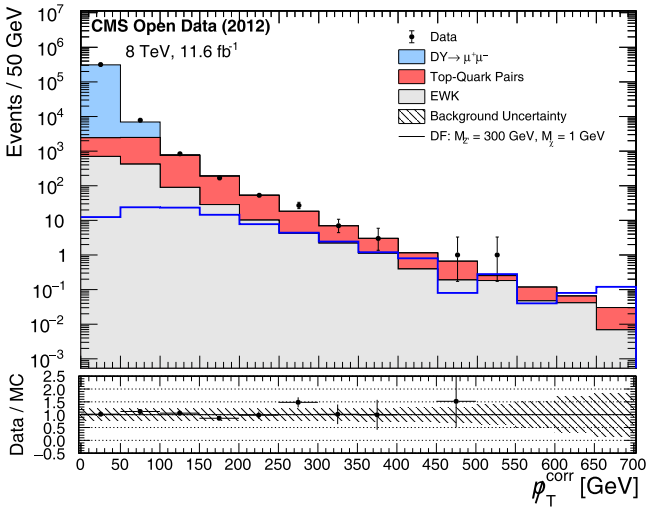

Fig. 2. (color online) Distribution of the missing transverse momentum after the preliminary selection for the CMS data, expected SM backgrounds, and DF scenario with $M_{Z'} = 300$ GeV and $M_{\chi_1} = 1$ GeV. The lower band shows the ratio between the data and simulation, and the shaded region corresponds to the statistical and systematic uncertainties in the predicted backgrounds, added in quadrature.

cuts have been applied. These tight cuts are based on four variables: the first variable is related to the invariant mass of the dimuon; we confined the invariant mass of the dimuon into a small region around the mass of Z' expressed as $(0.9 \times M_{Z'}) < M_{\mu^+\mu^-} < (M_{Z'} + 25)$. The second variable is $\Delta\phi_{\mu^+\mu^-,\vec{p}_T^{\,corr}}$, which is defined as the difference in the azimuth angle between the dimuon direction and missing transverse momentum direction (i.e., $\Delta\phi_{\mu^+\mu^-,\vec{p}_T^{\,corr}} = |\phi^{\mu^+\mu^-} - \phi^{miss}|$); it was selected to be greater than 2.6 rad. The third variable is the relative difference between dimuon p_T and missing transverse momentum ($|p_T^{\mu^+\mu^-} - \not{p}_T^{corr}|/p_T^{\mu^+\mu^-}$); it was selected to be less than 0.6. Finally, we introduced a requirement on the distance between the two muons in the (η, ϕ) plane: $\Delta R < 3$, where $\Delta R = \sqrt{(\Delta\eta)^2 + (\Delta\phi)^2}$. These tight cuts were applied to strongly decrease the SM backgrounds.

The sources of systematic uncertainties are related to the detector and theoretical framework. Some of these sources, considered in the presented results, are dis-

cussed next. The uncertainty in the evaluation of the integrated luminosity of the 2012 data recorded by the CMS detector was estimated to be 2.6% [50]. There was a 3% uncertainty related to the detector acceptance and reconstruction efficiency [35]. The uncertainty in the energy scale for particles with low energies (unclustered energy) was 10%, in addition to 2%−10% and 6%−15% uncertainties related to the jet energy scale and jet energy resolution, respectively. These uncertainties have a direct impact on the measurement of the missing transverse momentum [29]. The uncertainty in the transverse momentum resolution was 5%, and the uncertainty from the transverse momentum scale per TeV due to misalignment in the geometry of the CMS detector [35] was 5% as well. A 4.5% uncertainty related to the PDF choice of the DY process [35] was estimated in the present analysis; a 5% uncertainty related to the PDF for the WW process and 6% for the WZ process are also included.

V. RESULTS

The analytical procedure employed in this study follows a shape-based analysis where the variable used to discriminate the signal from the background is the missing transverse momentum distribution ($\not{p}_T^{\rm corr}$). This is justified by the fact that $\not{p}_T^{\rm corr}$ is much higher for the signal process than for the background process. The distribution of missing transverse momentum after the application of the final event selection is illustrated in Fig. 3. The observed data are in good agreement with the simulated backgrounds within the statistical and systematic uncertainties. The event yields passing the final analytical selection for each of the SM backgrounds, DF model (with $M_{Z'}$ = 300 GeV,M_{χ_1} = 1 GeV), and CMS open data corresponding to an integrated luminosity of 11.6 fb^{-1} are presented in Table 6.

To statistically interpret our results, we performed frequentist analysis (CL) [51] with profile likelihood-ratio test statistics [52] to derive exclusion limits on the product of signal cross sections and branching ratio Br($Z' \to \mu\mu$) at 95% confidence level.

These limits were applied separately for the different signal hypotheses at different masses of Z' and χ_1. To obtain the ±1 and ±2 sigma bands around the expected limit, pseudo-experiments with the background as only hypothesis was used. The nuisance parameters were randomely varied within the post fit constraints of the ML fit to the data.

A limit was set on the cross section times branching ratio Br($Z' \to \mu\mu$) for the DF scenario, as shown in Fig. 4 for the light dark sector masses. The blue solid line represents the cross section theoretically predicted as a function of Z' mass at a fixed DF mass (M_{χ_1} = 1 GeV). No significant deviation from the SM was observed in any of the studied mass points. Based on Fig. 4, the Z' production was excluded in the mass range between 238 − 524 GeV from the observed data and between 247 − 510 GeV from the expected median. For the DF scenario, the limit set on the cross section times branching ratio is presented in Fig. 5 as a function of the mediator's masses $M_{Z'}$ and masses of light DF M_{χ_1}. The observed exclusion is limited to a narrow region where M_{χ_1} is less than 25 GeV.

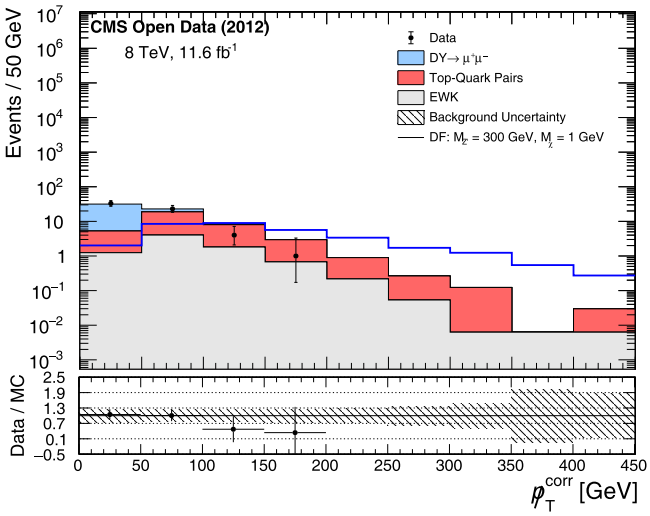

Fig. 3. (color online) Distribution of the missing transverse momentum after final analysis selection cuts for the expected background and observed events in the data of the $Z' \to \mu^+\mu^-$ channel. One signal benchmark corresponding to the DF scenario with $M_{Z'}$ = 300 GeV is superimposed. The signal is normalized to the product of the cross section and β, where β represents the $Z' \to \mu^+\mu^-$ branching fraction. The statistical and systematic uncertainties, added in quadrature, are presented by the hatched band. The ratios of the data and sum of all the SM backgrounds are shown in the bottom panel.

Table 6. Number of events satisfying the criterion of event selection for each SM background; the CMS open data correspond to an integrated luminosity of 11.6 fb^{-1} and the DF scenario signal with coupling constants $g_{\rm DM}$ = 1.0, $g_{\rm SM}$ = 0.1, and M_{χ_1} = 1 GeV. The total uncertainty, including the statistical and systematic components, is also indicated.

Process	No. of events
DY → $\mu^+\mu^-$	30.9 ± 8.3
$t\bar{t}$ + jets	28.3 ± 6.8
WW + jets	7.3 ± 1.8
WZ + jets	0.7 ± 0.2
ZZ → 4μ	0.04 ± 0.01
Sum Bkgs	67.2 ± 16.2
Data	61
DF signal (at $M_{Z'}$ = 300 GeV)	36.3 ± 8.8

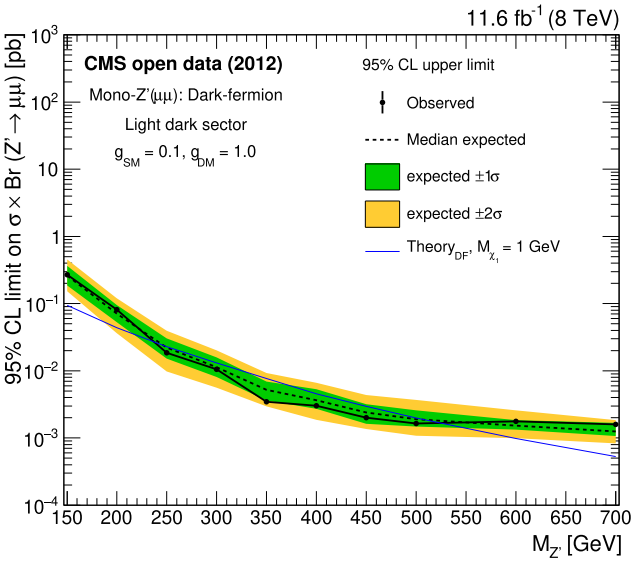

Fig. 4. (color online) Observed and expected upper limits on the cross section times branching ratio as a function of mediator's mass for a DF mass of $M_{\chi_1} = 1$ GeV at 95% CL. The blue line represents the DF scenario with $M_{\chi_1} = 1$ GeV.

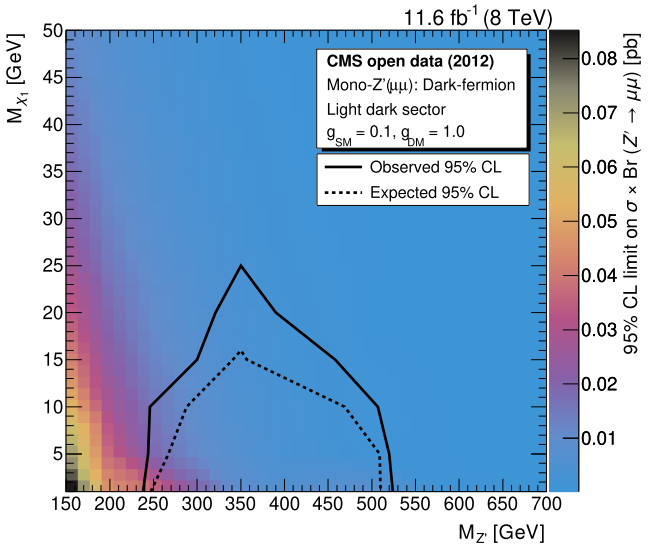

Fig. 5. (color online) Exclusion limits at 95% CL applied on the cross section times branching ratio for variations of pairs of the free model parameters ($M_{Z'}$ and M_{χ_1}). The filled region indicates the observed upper limit. The solid black curve indicates the observed exclusions for the nominal Z′ cross section, while the dotted black curve indicates the expected exclusions.

VI. SUMMARY

A search for DF particles was conducted. This search was based on the mono-Z' model in association with a heavy neutral gauge boson, Z'. We used a set of samples from proton-proton collisions released by the CMS open data project corresponding to an integrated luminosity of 11.6 fb^{-1} during RUN I. Results from the muonic decay mode of Z' were discussed along with its statistical and systematic combinations for the LV scenario. No significant deviation from the standard model prediction was observed. The 95% CL upper limits were set on the cross section times branching ratio (expected and observed), based on the mono-Z' model for the LV scenario. These limits constituted the most stringent limits on the parameters ($M_{Z'}$ and M_{χ_1}) of this scenario to date, thereby fixing the values of the coupling constants to $g_{\rm DM} = 1.0$, $g_{\rm SM} = 0.1$. For the LV scenario with a light dark sector mass assumption, a small region where the mass of DFs (M_{χ_1}) is less than 25 GeV was excluded. For $M_{\chi_1} = 1$ GeV, the corresponding excluded range of $M_{Z'}$ was 238 − 524 GeV from the observed data and 247 − 510 GeV from the expected median.

ACKNOWLEDGMENTS

We would like to thank Tongyan Lin, co-author of [13], *for providing us with the UFO model files, helping us with the generation of the signal events, and cross-checking the results.*

DATA AVAILABILITY STATEMENT

The data sets used and analyzed during the current study are available in the CERN's open data portal at the following URL links:

http://opendata.cern.ch/record/7741.
http://opendata.cern.ch/record/9577.
http://opendata.cern.ch/record/9971.
http://opendata.cern.ch/record/9983.
http://opendata.cern.ch/record/10071.
http://opendata.cern.ch/record/6021.
http://opendata.cern.ch/record/6047.

References

[1] Planck Collaboration, Astron. Astrophys. **594**, A13 (2016), arXiv:1502.01589[iNSPIRE-HEP]
[2] Planck Collaboration, *Planck 2018 results. VI. Cosmological parameters* , A&A **641**, A6 (2020), arXiv: 1807.06209[astro-ph.CO]
[3] C. Lage and G. Farrar, JCAP **2015**, 038 (2015)
[4] G. Bertone, D. Hooper, and J. Silk, Phys. Rept. **405**, 279 (2005), arXiv:hep-ph/0404175[iNSPIRE-HEP]
[5] Scherrer, Robert J. and Turner, Michael S., Phys. Rev. D **33**, 1585 (1986)
[6] F. Halzen and A. D. Martin, *Quarks And Leptons: An Introductory Course In Modern Particle Physics*,

(1984), ISBN: 0471887412, 9780471887416
[7] P. Langacker, *The standard model and beyond*, (2010). ISBN: 9781420079067
[8] M. Beltran *et al*., *Maverick dark matter at colliders*, arXiv: 1007/JHEP09(2010)037
[9] CMS Collaboration, Phys. Rev. D **97**, 092005 (2018), arXiv:1712.02345[hep-ex]
[10] CMS Collaboration, JHEP. **10**, 073 (2017), arXiv:1706.03794v2[hep-ex]
[11] CMS Collaboration, JHEP **03**, 025 (2020), arXiv:1908.01713v2[hep-ex]
[12] Krovi AniruDF, Low Ian, and Zhang Yue, JHEP **10**, 026 (2018), arXiv:1807.07972[hep-ph]
[13] Marcelo Autran and Kevin Bauer, Phys. Rev. D **92**, 035007 (2015), arXiv:1504.01386[hep-ph]
[14] Paul Langacker, Rev. Mod. Phys. **81**, 1199 (2009), arXiv:0801.1345[hep-ph]
[15] Cheng-Wei Chiang, Takaaki Nomura, and Kei Yagyu, JHEP **05**, 106 (2014), arXiv:1402.5579[hep-ph]
[16] Digesh Raut, *Gauged U(1) extension of the SM and Phenomenology*, PhD U. Alabama, Tuscaloosa (2018), [iNSPIRE-HEP].
[17] R. Foot, X. G. He, H. Lew *et al*., Phys. Rev. D **50**, 4571 (1994), arXiv:9401250[hep-ph]
[18] ATLAS Collaboration, JHEP **10**, 180 (2018), arXiv:1807.11471[hep-ex]
[19] S. Elgammal, M. Louka, A. Y. Ellithi *et al*., Eur. Phys. J. Plus **138**, 6 (2023)
[20] CMS Collaboration, Software Framework for CMS Open Data Analysis
[21] Aram Apyan, William Cuozzo, Markus Klute *et al*., JINST 15 (2020), arXiv:1907.08197[hep-ex]
[22] CMS Collaboration, Phys. Rev. D **93**, 052011 (2016), arXiv:1511.09375[hep-ex]
[23] CMS Collaboration, Eur. Phys. J. C **81**, 13 (2021), arXiv:2008.04735[hep-ex]
[24] A. Albert *et al*., *Recommendations of the LHC Dark Matter Working Group: Comparing LHC searches for heavy mediators of dark matter production in visible and invisible decay channels*, CERN-LPCC-2017-01, arXiv: 1703.05703v2[hep-ex]
[25] Johan Alwall, Michel Herquet, Fabio Maltoni *et al*., JHEP **06**, 128 (2011)
[26] M. Mulders (the CMS Collaboration), Nucl. Phys. B **172**, 205 (2007)
[27] CMS Collaboration, JINST **7**, P10002 (2012), arXiv:1206.4071[physics.ins-det]
[28] CMS Collaboration, *Particle-Flow Event Reconstruction in CMS and Performance for Jets, Taus, and MET*, Tech. Rep. CMS-PAS-PFT-09-001, CERN, Geneva, Apr, 2009
[29] CMS Collaboration, JINST **10**, P02006 (2015), arXiv:1411.0511[physics.ins-det]
[30] CMS Collaboration, JINST **12**, P10003 (2017), arXiv:1706.04965v2[physics.ins-det]
[31] http://opendata.cern.ch/docs/cms-physics-objects-2011.
[32] CMS Collaboration (2016), *CMS Software Version 5_3_32 (CMSSW_5_3_32)*, CERN Open Data Portal
[33] Torbjon Sjostrand, Stephen Mrenna, and Peter Skands, JHEP **05**, 026 (2006), arXiv:hep-ph/0603175
[34] CMS Collaboration (2018), *Simulated pile-up dataset MinBias_TuneZ2star_8TeV-pythia6 in GEN-SIM format for 2012 data*, CERN Open Data Portal
[35] CMS Collaboration, JHEP **04**, 025 (2015), arXiv:1412.6302[hep-ex]
[36] CMS Collaboration, *CMS list of validated runs for primary datasets of 2012 data taking,*, CERN Open Data Portal
[37] Simone Alioli, Paolo Nason, Carlo Oleari *et al*., JHEP **06**, 043 (2010)
[38] Simone Alioli, Paolo Nason, Carlo Oleari *et al*., JHEP **07**, 060 (2008)
[39] CMS Collaboration, *Simulated dataset DYToMuMu_M-20_CT10_8TeV-powheg-pythia6 in AODSIM format for 2012 collision data*, CERN Open Data Portal
[40] CMS Collaboration, *Simulated dataset TTJets_FullLeptMGDecays_8TeV-madgraph in AODSIM format for 2012 collision data*, CERN Open Data Portal
[41] John M. Campbell and R.K. Ellis, Nucl. Phys. B Proc.Suppl. **205-206**, 10 (2010)
[42] CMS Collaboration, *Simulated dataset WWJetsTo2L2Nu_TuneZ2star_8TeV-madgraph-tauola in AODSIM format for 2012 collision data*, CERN Open Data Portal
[43] CMS Collaboration, *Simulated dataset WZJetsTo3LNu_TuneZ2_8TeV-madgraph-tauola in AODSIM format for 2012 collision data*. CERN Open Data Portal
[44] CMS Collaboration, *Simulated dataset ZZTo4mu_8TeV-powheg-pythia6 in AODSIM format for 2012 collision data*, CERN Open Data Portal
[45] CMS Collaboration, *SingleMu primary dataset in AOD format from Run of 2012 (/SingleMu/Run2012B-22Jan2013-v1/AOD)*. CERN Open Data Portal
[46] CMS Collaboration, PoS LHCP **2019**, 260 (2019)
[47] CMS collaboration, *SingleMu primary dataset in AOD format from Run of 2012* (/SingleMu/Run2012C-22Jan2013-v1/AOD). CERN Open Data Portal
[48] CMS Collaboration, JHEP **1105**, 093 (2011), arXiv:1103.0981[hep-ex]
[49] https://twiki.cern.ch/twiki/bin/view/CMSPublic/SWGuideMuonIdHighPT_Muon.
[50] CMS Collaboration, *CMS Luminosity Based on Pixel Cluster Counting - Summer 2013 Update*, CMS Physics Analysis Summary CMS-PAS-LUM-13-001 (2013)
[51] A. L. Read, J. Phys. G **28**, 2693 (2002)
[52] G. Cowan *et al*., Eur. Phys. J. C **71**, 1554 (2011) [Erratum: Eur. Phys. J. C **73**, 2501 (2013)], arXiv: 1007.1727 [physics.data-an]